SOFT ROBOTICS
Volume 00, Number 00, 2023

DOI: 10.1089/soro.2022.0198

SoRo
Soft Robotics





# Multimodal Locomotion in a Soft Robot Through Hierarchical Actuation

Qifan Yu and Nick Gravish

## Abstract

Soft and continuum robots present the opportunity for extremely large ranges of motion, which can enable dexterous, adaptive, and multimodal locomotion behaviors. However, as the number of degrees of freedom (DOF) of a robot increases, the number of actuators should also increase to achieve the full actuation potential. This presents a dilemma in mobile soft robot design: physical space and power requirements restrict the number and type of actuators available and may ultimately limit the movement capabilities of soft robots with high-DOF appendages. Restrictions on actuation of continuum appendages ultimately may limit the various movement capabilities of soft robots. In this work, we demonstrate multimodal behaviors in an underwater robot called ''Hexapus.'' A hierarchical actuation design for multiappendage soft robots is presented in which a single high-power motor actuates all appendages for locomotion, while smaller low-power motors augment the shape of each appendage. The flexible appendages are designed to be capable of hyperextension for thrust, and flexion for grasping with a peak pullout force of 32 N. For propulsion, we incorporate an elastic membrane connected across the base of each tentacle, which is stretched slowly by the high-power motor and released rapidly through a slip-gear mechanism. Through this actuation arrangement, Hexapus is capable of underwater locomotion with low cost of transport (COT = 1.44 at 16.5 mm/s) while swimming and a variety of multimodal locomotion behaviors, including swimming, turning, grasping, and crawling, which we demonstrate in experiment.

**Keywords:** multifunctional soft robot, underwater robot, multi-modal locomotion

## Introduction

In mobile robot applications such as exploration in unstructured environments, it can be advantageous for robots to execute multiple different locomotion modalities, a behavior called multimodal locomotion.[1–3] Recent robots have demonstrated multimodal capabilities, including combinations of aerial, aquatic, and on-land locomotion in single platforms.

Multimodality can arise from combining mode-specific components on a robot that achieve desired locomotion modes. For example, a robot with propeller and feet can both fly and climb,[4,5] a robot with a tail and legs can swim and walk,[6] and a robot with legs and wings can both glide and walk.[7] Alternatively, robot components (appendages for example) can be co-opted for multiple locomotion functions (multifunctional), such as legs that enable walking and swimming,[8] snake-like bodies that enable ground slithering

Department of Mechanical and Aerospace Engineering, University of California San Diego, San Diego, California, USA.

and climbing,[9] and self-reconfigurable modules that enable slithering, crawling, rolling, and object grasping.[10–14] Multifunctionality in appendages requires multiple degrees of freedom (DOF) of motions, as well as actuation capabilities that can augment the behavior of limbs and drive different movements for different environments.

Soft robots, often composed of appendages and bodies that can deform continuously and elastically, present an opportunity for high-DOF motions that can enable dexterous, adaptive, and multimodal locomotion behaviors.[15,16] Existing soft robots with multi-DOF actuations exhibit multimodal locomotion as well as compliant interaction with the environment.[17–22] However, effectively actuating such high-DOF systems remains a considerable challenge. This is especially the case for mobile robots, which must carry around all power and actuation sources.

An exemplary application for multimodal locomotion is in underwater robots that must safely and independently navigate in complex environments, such as near the seafloor, within kelp beds and coral reefs, or in the shallow inter-tidal zone.[1] Soft multifunctional robots present a unique opportunity for underwater, multimodal locomotion as their soft bodies inhibit potential damage or entanglement to the environment due to rigid components like rotary propellers. However, most modern soft underwater robots have relatively few actuators (1 to 2 per appendage),[23–30] which may limit the full potential of their soft bodies and fundamentally limit their functionalities. Some underwater robots use multiple actuators and present different modes of locomotion[31–35] and the potential for small object grasping.[8,36–41] However, independent operation in complicated and unstructured environments still remains a challenge due to the large power consumption for these systems.

In robot design, the form factor, bandwidth, and power output for an actuator are major factors for robot performance. This is particularly challenging for multi-DOF robotic systems because performance and form factor of actuators such as traditional electromagnetic motors are closely coupled, so their power output tends to decrease as their sizes decrease. Thus, to accommodate higher DOF in a confined space or mass, often, we are restricted to smaller volumes for actuation and thus weaker actuators.[42] To circumvent the tradeoff between power and number of DOF, new designs that differentiate (or diversify) actuators' power outputs in rigid multi-DOF robotic systems[42,43] have shown maintained power output and position control, as a result of using both high-power ''macro'' actuators and low-inertia, but high-precision ''mini'' actuators. In terms of underwater robotic system, this differentiation of actuator form factors that strategically divide workloads suggests potential improvement in both robot efficiency and multifunctionality.[44]

In this work, we take inspiration from the biomechanics and locomotion of the octopus into the development of a six-arm soft robot, Hexapus. To achieve dexterous and multimodal arm movements, while maintaining efficient and high-power swimming behaviors, Hexapus implements a ''hierarchical actuation'' design that uses small low-power motors to strategically allocate and augments the action of a high-power motor across all appendages. Using six soft arms controlled by one large high-power motor and six smaller low-power motors, Hexapus demonstrates a wide range of locomotion, including forward and backward swimming, 3D navigation, grasping, object transporting, anchoring, and crawling (Fig. 1). Hexapus demonstrates efficient locomotion (cost of transport [COT] as low as 1.44) and dexterous movements, enabling high maneuverability, endurance to unexpected external events, as well as eco-friendly interactions with environments.

## System Design and Fabrication

Similar to octopus, Hexapus consists of six soft arms and a head chamber that contains the control electronics and actuators (Fig. 2b). We began with an overall size target of 30 cm in length for the robot so that it would be large enough to use standard fabrication methods, while still small enough to move in unstructured seafloor environments and to grasp on to objects. From the overall size specification, the design process consisted of choosing appropriate actuators given, the power limits and form factor of the robot.

Incorporating additional design decisions, including an elastic energy release mechanism and tendon-driven appendages, we designed Hexapus as a multifunctional soft

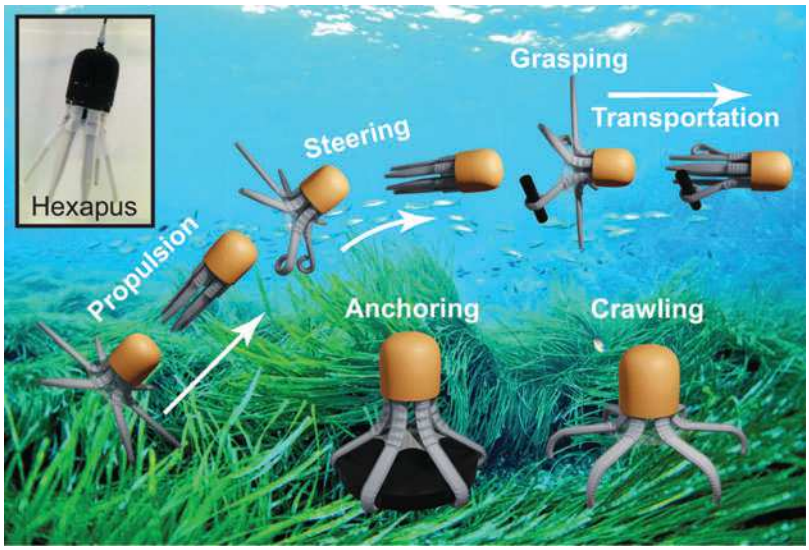


**FIG. 1.** Envisioned underwater robot capable of multimodal locomotion. Capabilities include propulsion, turning, grasping, transportation, crawling, and anchoring. *Inset* shows the fabricated underwater robot, Hexapus, proposed in this article.

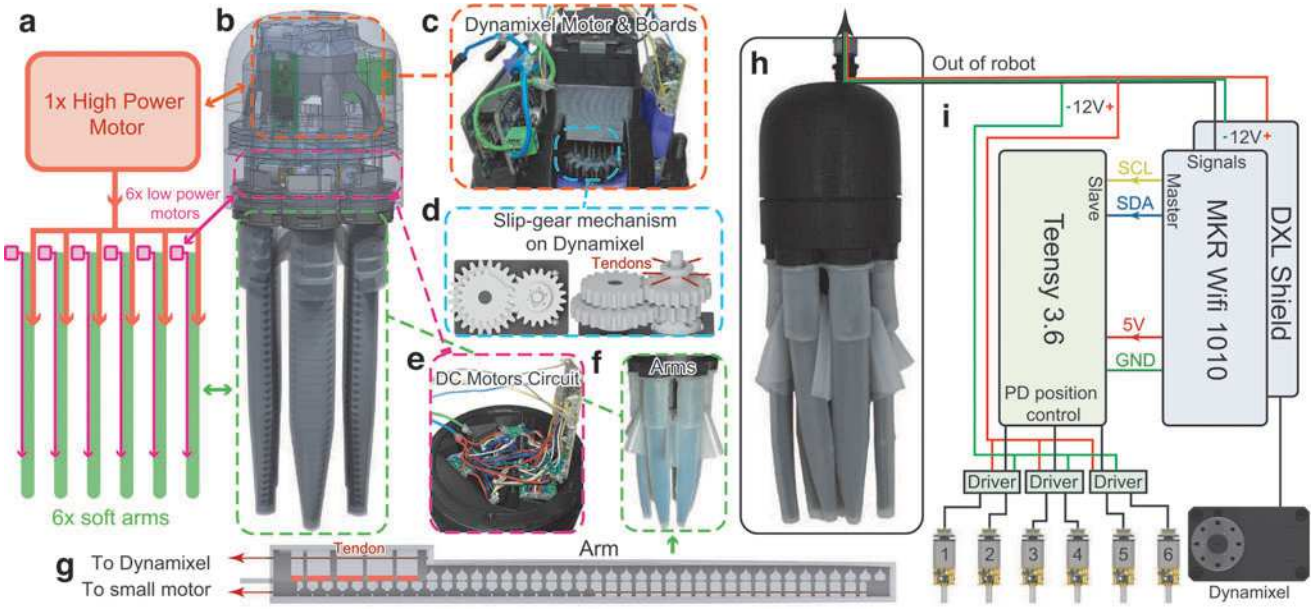


**FIG. 2.** Robot designs and integration. **(a)** Schematic showing hierarchical actuation design, where a high-power motor actuates one side of all six arms of the robot and six low-power motors actuate the other side of six arms separately, giving the robot seven DOF in total. **(b)** Rendered overview of Hexapus and its internal view. **(c)** *Top* compartment layout of the head chamber. **(d)** Slip-gear mechanism that realizes the elastic release of arms. **(e)** *Bottom* compartment of Hexapus' head, where circuitry, low-power DC motors, and drivers reside. **(f)** Assembled silicone membrane, weight, and arms. **(g)** Underactuated tendon-driven arm design. Dynamixel motor actuates the *top* tendon (*red*) and enables propulsion through hyperextension; low-power motor actuates *bottom* tendon and enables tip curling or flexion. **(h)** Photograph of the assembled robot. **(i)** Wiring diagram for motor controls. External signals and power are fed from a waterproof connector. DOF, degrees of freedom.



robot that uses ''macro-mini'' inspired actuation strategy—which we call hierarchical actuation that is described in Actuation section. The entire robot weighs 1.32 kg and is 33 cm long and 10 cm wide in diameter and when the arms are fully open, Hexapus is $13 \pm 1$ cm long and $58 \pm 4$ cm wide. In the following sections, we describe the design and fabrication details of each component of Hexapus.

### *Head*

The head section of Hexapus is a waterproof chamber that contains all electronics, including control boards, drivers, and motors (Fig. 2b). Six arms and a weight chamber containing a 330 g stainless steel ballast are fixed at the bottom of the head chamber. The mass ensures Hexapus is neutrally buoyant with center of mass at the center of buoyancy.

The fabricated head chamber consists of a lid and a chassis where arms mount, both of which are 3D printed using polylactic acid (PLA). Two o-rings are attached in interfaces between any two parts—between lid and chassis and between chassis and each arm. The exterior of the head chamber and weight chamber is sprayed with Flex Seal® coating, a waterproof sealant, to prevent water seepage.

### *Arms*

Each soft arm or tentacle of Hexapus has a tapered profile (Fig. 3a) that enables the tip to manipulate dexterously with low drag, while the base segments of the arms still have large surface area to produce thrust. To further enhance swimming thrust, a 1 mm thick silicone hexagon-shaped membrane (Supplementary Fig. S2a) is attached to the six arms below the weight chamber, increasing the thrust.[45] Each arm is capable of bending in hyperextension (opening up the arms for thrust) and tip flexion (closing for grasping), as well as combinations of these two actuation modes (Fig. 3b).

The internal structures of the arms are fabricated using a hybrid fabrication approach called flexoskeleton printing[46,47] where a fused deposition modeling 3D-printer (Prusa i3 MK3S+) is used to print rigid PLA onto a soft, but inextensible polycarbonate film to achieve flexible tendon-driven structure. Each of the six arms consists of two internal flexoskeleton structures that each has tendon guides and ridge-shaped supports to brace the outer silicone skin (Fig. 3a). The front flexoskeleton consists of a tendon-actuated hyperextension actuation segment near its base. To ensure sufficient storage and efficient release of energy (high stiffness and low hysteresis), two short 0.4 mm diameter elastic Nitinol rods are embedded into the actuation segment of the front flexoskeleton (Fig. 3a). In addition, the fatigue resistance of flexoskeleton structures has been studied in Jiang et al.[46]

Finally, a soft silicone shell encases the inner flexoskeleton structure. Each of the six silicone shells is cast using Dragon Skin™ 10A on a 3D printed sheath-and-core mold; the 1 mm thick membrane is cast using a 3D printed mold and is attached to arms using Sil-Poxy® adhesive (molds shown in Supplementary Fig. S1, geometries shown in Supplementary Fig. S2). The silicone shell design (1) ensures watertightness, (2) creates a smooth interface with water to

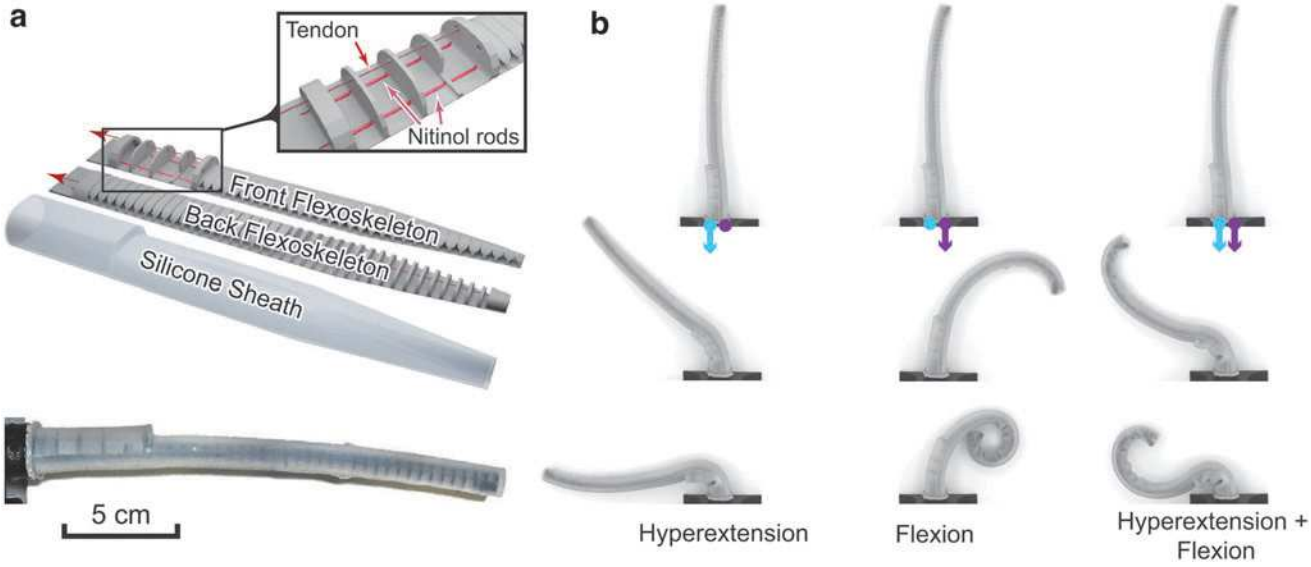


**FIG. 3.** Arm design and capabilities. **(a)** Rendered front and back flexoskeleton layers that are bonded together and which comprise the arm inner structure. The front flexoskeleton layer faces outward from Hexapus' central axis, while the back flexoskeleton layer faces inward toward Hexapus' central axis. The silicone sheath encases the inner flexoskeleton structure. The front flexoskeleton layer base contains two Nitinol rods for increased stiffness and elastic resilience (*inset*). **(b)** Three examples of arm actuation from *left* to *right columns*. Hyperextension (*left*), flexion (*middle*), and combination of hyperextension and flexion (*right*). See Supplementary Video S1.

minimize drag, (3) integrates two flexoskeleton structures so two are not separated, and (4) results in nearly neutrally buoyant arms.

### *Actuation*

Similar to the tendon-driven ''macro-mini'' actuation design,[42] the design of the power system in Hexapus is inspired by the octopus, which is known to have powerful mantle muscles for propulsion, and high DOF but weaker musculature on their tentacles for manipulation.[48] We use hierarchical actuation, which consists of three actuation methods as shown in Figure 2a, to drive the multimodal locomotion capabilities of Hexapus, as shown in Figure 4 (Supplementary Video S1). A single high-power source accompanied with an elastic energy release mechanism for locomotion, and six low-power sources for multifunctional behaviors. Compared to using identical actuators, this hierarchical design enables compact placement of motors that fit within our body volume constraints and power output constraints.

In our design, we considered only electromagnetic (DC) motors for driving arms with tendons, but similar design may

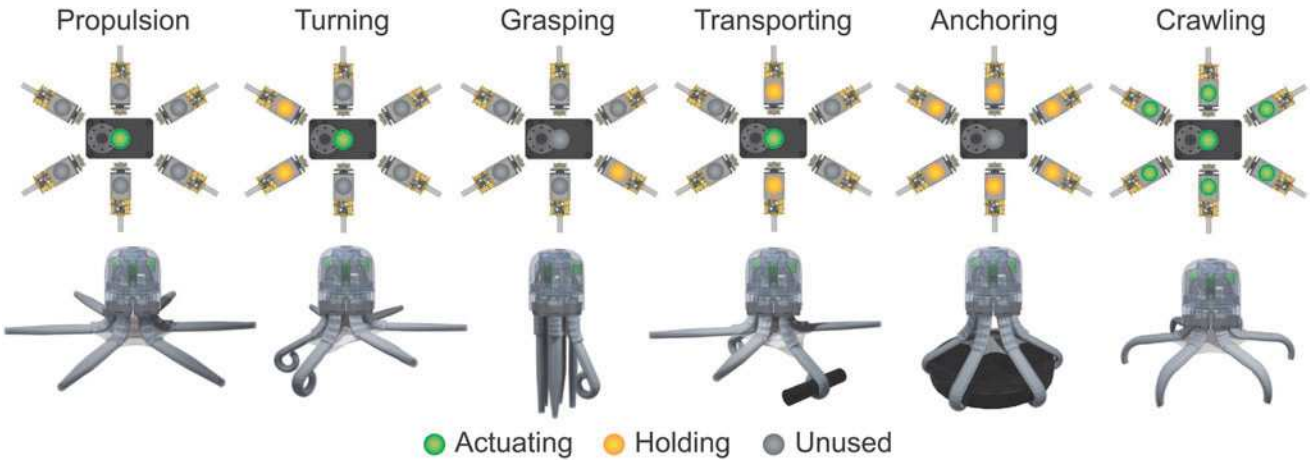


**FIG. 4.** Multifunctionality. Upon actuation of the Dynamixel motor (hyperextension), Hexapus can propel itself forward and backward, as well as performing tasks, including turning and transporting by holding small radius grasps at arms' tips. Stationary operations such as grasping and anchoring are also enabled by holding objects of different sizes using curled-in arms (flexion). Crawling is enabled when all motors are used for actuation.

extend to other modes of actuation. Many soft robots are currently actuated through pneumatic and hydraulic networks within the body.[16] However, the majority of these systems to date still use electromagnetic motors for pressure generation. Furthermore, unstable buoyant forces and sealing for these modes of actuation make their operations underwater challenging. Actuators such as shape memory alloys, liquid crystal elastomers, or other smart actuators that can be embedded directly at the site of actuation may circumvent the scaling issues. However, such ''local'' actuators are often limited in their energetic efficiency, operational bandwidth, and force/torque output.[49,50]

High-power motor actuation for arm hyperextension. A large servo motor (Dynamixel motor XL430-W250-T; $30\times40\times50$ mm) is used to actuate all arms' hyperextension simultaneously through six tendons in parallel and a 2:1 slip-gear system (Fig. 2d, g). The Dynamixel motor is controlled under velocity mode with position feedback.

Elastic release for forward thrust. To enable passive return of the arms under elastic recoil, we added an energy release ''slip-gear'' mechanism for forward propulsion performance. Four out of 20 teeth on the compound gear in the 2:1 gear system are removed to produce a cyclic demeshing between two gears.

This mechanism enables high-power output by releasing arms rapidly during the releasing stroke (when gears demesh), while allowing position control of arms in their operating range (when gears mesh) (Fig. 2d and Supplementary Video S1). A low stiffness torsional spring is attached along the shaft to avoid incomplete recovery of the slip-gear mechanism due to friction. The maximum swimming amplitude of the arms in hyperextension is set to 100°; the slight over-recovery of the slip-gear mechanism lowers it to ~90°–100° in most cases. When the gear system is meshed, the elasticity of the soft arms plus the high-power motor allow arms to perform bidirectional movement at their bases. To simulate the robot's forward swimming motion, we propose a two dimensional finite element analysis (FEA) as discussed in Supplementary Materials. The model inputs are shown in Supplementary Figure S4, the result arm profile is shown in Figure 5b, and the swimming profile is shown in Figure 6b.

Low-power motor actuation for arm flexion. Six high-gear-ratio (380:1) and small ($10\times12\times40$ mm) Pololu brushed DC motors under position control actuate the flexion of the arms. Each of these low-power motors actuates a tendon connected to the tip of the back flexoskeleton. Pulling this tendon results in a small-radius inward curl that begins at the arm's tip and propagates down the arm toward the base due to the stiffness gradient design of the arm.[47] Thanks to the high-ratio gearboxes and low backdrivability, the motors are able to maintain their curling shape with negligible power consumption. Thus, these less efficient actuators are run at very low duty factors.

### *Control*

An Arduino MKR WiFi 1010 board shown in Figure 2c is used to control all motors. The Dynamixel motor is velocity controlled with position monitored by a Dynamixel shield that has serial communication with the MKR board (Fig. 2i). Six DC motors are driven by three DC motor drivers that are controlled by proportional differential controllers coded in Teensy 3.6 board, which has I2C communication with the MKR board. Power supply for all motors (12 V) and a data wire that controls the MKR board are input from a waterproof connector on top of the head chamber. Future untethered design can be easily incorporated into the current control system by adding batteries in place of the steel ballast and inputting commands through WiFi module on the MKR board.

## Results

### *Flexoskeleton arm performance*

In each arm, there are three components providing elasticity: (1) the internal flexoskeleton structure, (2) superelastic

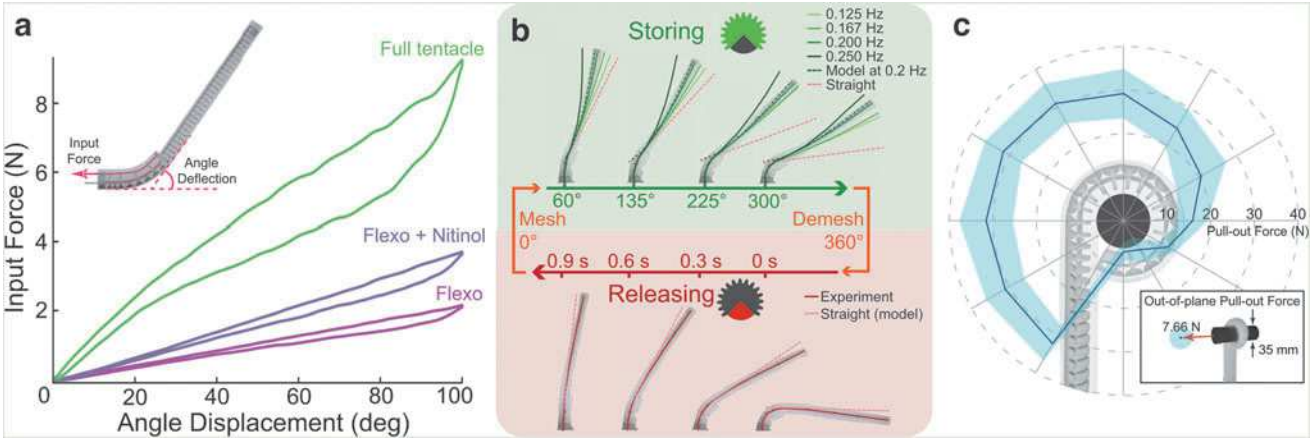


**FIG. 5.** Arm actuation. Results from arm performance experiments. **(a)** Comparison of tendon force and bending angle displacement for the entire arm with sheath (*green*, *top curve*), the front flexoskeleton with nitinol wire (*purple*, *middle curve*), and the flexoskeleton alone (*pink*, *bottom curve*). *Inset* shows measurement example. **(b)** Thrust cycle at different frequencies of Dynamixel actuation. Different drag under different actuation frequencies induces different profiles of arm during storing stroke, while front flexoskeleton is jammed and arm profile is almost straight during releasing stroke. The forward propulsion model computes arm profile (*green dashed line*) during storing stroke using finite element analysis (FEA), while the model assumes straight arm profile (*red dashed line*) during releasing stroke due to flexoskeleton jamming. **(c)** Pull-out force of one arm in different directions. Each data point consists of 15 trials with line representing average and shaded region the standard deviation.

nitinol wires placed along the hyperextension bending region, and (3) the silicone sheath. The actuation tendon for hyperextension was attached to a force sensor and displacement stage and we measured tendon force versus bending angle of a single arm (Fig. 5a). The flexoskeleton (flexo) alone and the flexoskeleton+nitinol configurations displayed a linear force-displacement curve with low energy loss (flexo: 6.2%, flexo+nitinol: 5.2% energy loss). The addition of nitinol wires to the arm increased stiffness by 70%. When the silicone skin is added to the arm, the overall stiffness increased by an additional 144% and shows hyperelastic profile, but the energy dissipation during the loading and unloading cycle increased to 21.6% energy loss.

To demonstrate and optimize the thrust capabilities during elastic actuation of the arms, we used the slip-gear actuation mechanism to load and release a single arm underwater across four loading rates (0.125, 0.167, 0.200, and 0.250 Hz) and tracked the arm deformation across a load-unload cycle. The arm bending profiles during loading and release are plotted in Figure 5b. As the loading rate increased, the arm began to experience larger flexion deformation because of larger fluid drag. A finite element model of the arm introduced in Supplementary Data was able to reasonably reproduce the loading and unloading deformation of the arm, indicating that a linear model of bending elasticity and fluid drag is sufficient to predict the fluid-structure interaction during loading and thrust. The arm bending during release was qualitatively the same for all loading actuation frequencies (Fig. 5b, bottom).

Finally, we performed a pull-out experiment on an arm to measure its grasping capability. The experiment consisted of curling arm's tip in flexion by 360° and grips on to a cylindrical object with a diameter of 3.5 cm. The object is then displaced along a straight line by a translation stage, while measuring the grasp force exerted on the cylinder. We varied the pull-out direction over a 360° range in 30° increments and repeated the experiment 15 times for each angle (results shown in Fig. 5c). The grasp force varied as a function of pull-out angle and was the largest (32 N) when the pull-out angle was oriented inwards and toward the arm base.

### *Forward and backward swimming*

Forward swimming allows Hexapus to swim and maneuver efficiently using the elastic storage and release for high efficiency movement. Backward swimming allows Hexapus to move with the arms facing toward the moving direction, thus enabling it to approach targets without the need for reorientation in between tasks (grasping, anchoring, or walking). To measure the forward swimming capabilities, we placed the neutrally buoyant robot vertically underwater and used four vertical guidewires to constrain it to move vertically. A waterproof camera in front of Hexapus monitors its vertical displacement.

In the forward swimming experiments, we varied the loading rate of the arms between 0.125 and 0.250 Hz using the Dynamixel motor only. The thrust stroke of Hexapus was generated through the elastic restoring force of the arms. An example of swimming profile at 0.2 Hz is shown in Figure 6b. A hydrodynamic model of forward propulsion similar to McHenry and

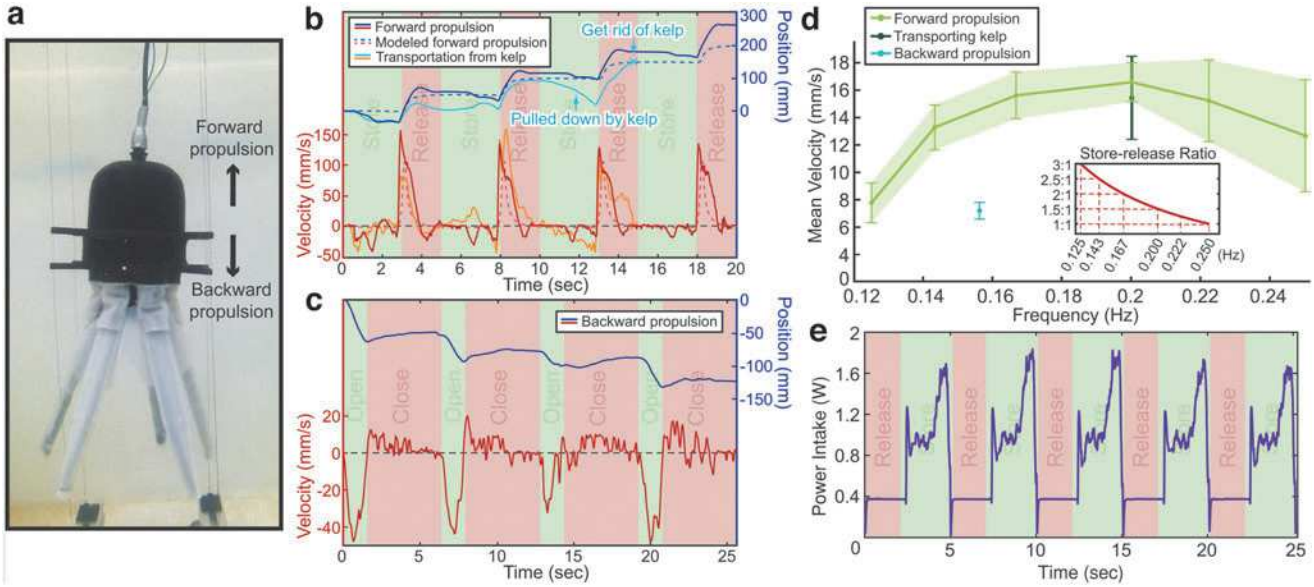


**FIG. 6.** Forward and backward swimming performance. **(a)** Underwater setup of Hexapus for forward and backward propulsion demonstration. Hexapus is constrained to move in one direction by four vertical guide wires. **(b)** Displacement and velocity profiles of 0.2 Hz forward swimming (*dark blue* and *red*), kelp sample transportation demonstration from a cluster of kelp (*light blue* and *orange*), and straight propulsion model result (*dashed blue* and *red*). **(c)** Displacement and velocity profile of 0.156 Hz backward swimming. **(d)** Mean velocity of forward propulsion (*light green*) at various frequencies, and straight kelp transportation velocity at 0.2 Hz (*dark green*), and backward swimming. Each data point consists of 15 cycles of propulsion. **(e)** Example trial power intake of the robot Hexapus during forward propulsion. The power intake starts to increase slightly after storing phase begins because the tendons being actuated are slack at the end of the release phase.

Jed[51] detailed in Supplementary Data is used to predict robot forward swimming profile (dashed lines in Fig. 6b).

In the backward swimming experiments, the Dynamixel motor is actuated up to the limit of the slip-gear demeshing point, but not past it. In a backward propulsion actuation sequence, the Dynamixel motor first opens the arms quickly (60°/s) and stops before the gears demesh (90°), and then it closes the arms slowly by actuating backward (20°/s). The drag difference between the storing and release strokes due to velocity difference allows Hexapus to propel backwards. An example of robot's backward swimming trajectory is shown in Figure 6c.

The mean forward swimming velocity of Hexapus was a nonmonotonic function of the actuation frequency (Fig. 6d). At low actuation frequency, the loading time of the arms dominated the actuation cycle and slowed the robot, while at high loading frequency, the increased backward drag during arm loading likely resulted in speed reduction. The optimal actuation frequency that maximized forward propulsion was around 0.2 Hz, which achieved a proficiency (speed per body length) of 0.11 $s^{-1}$.

An example of power intake of Hexapus during forward swimming is shown in Figure 6e. We found Hexapus' COT of 1.44[31] in free swimming trials by measuring the swimming velocity through an underwater camera and the power intake using a current sensor (INA219) at constant supply voltage. This value is relatively low compared to most octopus-inspired or jellyfish-like robots (>10 fromVillanueva et al.,[52] 2.94 from Ren et al.,[31] 2.9 from Cianchetti et al.[37]), and is close to COT of a small octopus (0.80 for a 40 g octopus[53]). The backward COT was measured to be 4.80 and is substantially larger than the forward case, demonstrating the effectiveness of elastic storage and release.

### *Turning*

Turning was implemented by curling specific arms in flexion such that during the swimming stroke, curled arms experience a reduction in drag. The drag difference across the robot body will result in a turning moment. To test the performance of this control method, we actuated a number (one to five) of adjacent arms into a curled shape (of ~360°) and then executed a single swimming cycle.

We use two parameters to characterize the turning performance: (1) the turning angle per cycle and (2) the steering accuracy (Fig. 7a). The turning angle is the relative angular change of robot's heading direction, and the steering accuracy is the azimuthal angle measured between the goal direction and the actual robot direction in spherical coordinates. To measure this performance, the robot's orientation and position were tracked in 3D using two cameras (in front and on top of Hexapus).

Averaged 3D trajectories of the robot's body are plotted in Figure 7b. Although the asymmetry of arms peaks when three arms on one side curl in, the turning angle maximizes when four arms are curled in and then there is a reduction when five arms are curled (Fig. 7d). Over all experiments, the steering accuracy was consistent and relatively small, yielding an ~15°steering error across all arm configurations (Fig. 7f).

### *Transportation and anchoring*

Grasping and transporting were demonstrated in a simulated kelp bed in a laboratory tank. Hexapus is constrained to move along a vertical axis by four constraining cables. Hexapus descends to the kelp bed under backward propulsion; when at the kelp bed, it actuates a single arm in flexion to encircle a strand of kelp, and finally it propels to the surface using forward propulsion (Supplementary Video S2). To maintain steering symmetry, the arm opposite to the grasping arm is also curled in flexion. At the optimal actuation frequency of 0.2 Hz, the forward transportation speed when Hexapus was grasping the kelp strands reduced by only 7.6% compared to free forward propulsion (Fig. 6a, d).

In addition to transporting objects, arm flexion can be used to anchor Hexapus onto the seafloor. To determine the effectiveness of the anchoring behavior, we performed experiments in a laboratory water tank on five simulated sea floor objects: (1) orange pipe coral, (2) lettuce coral, (3) branching coral, (4) a sea anemone (soft), and (5) sea kelp (soft). These objects were adhered to a weight and placed at the bottom of a

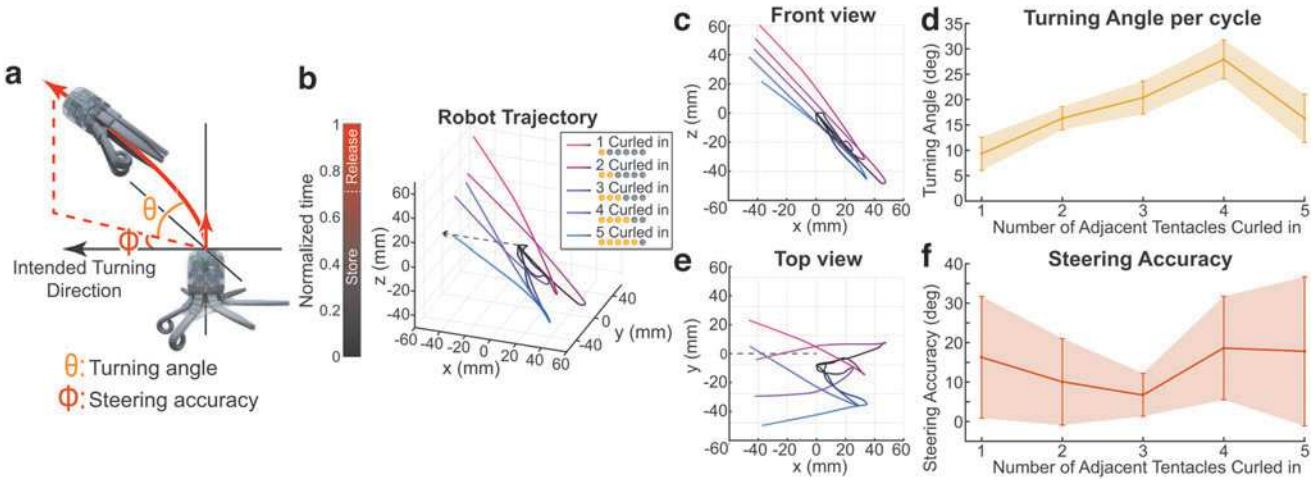


**FIG. 7.** Turning trajectory. **(a)** Illustration of turning angle and steering accuracy in one turning cycle. **(b)** Robot's positions as functions of time, three-dimensional space, and the number of arms curled in. **(c)** Front view of robot's position. **(d)** Turning angle per cycle of the robot calculated through its altitudinal orientation change after one cycle. **(e)** Top view of robot's position. **(f)** Steering accuracy per cycle of the robot calculated through its azimuthal orientation change after one cycle. For each number of curled-in arms, seven cycles of propulsion are tracked.

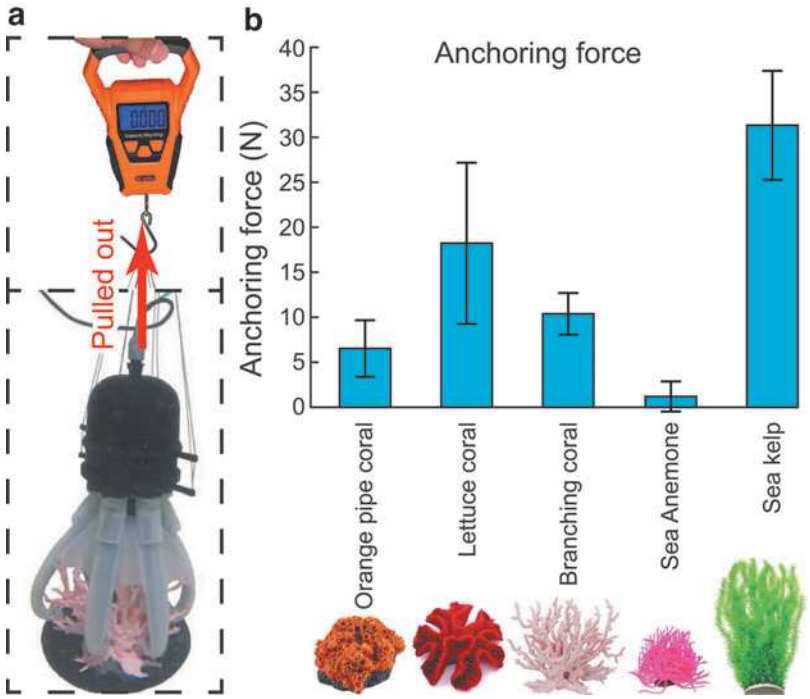


**FIG. 8.** Force required to pull Hexapus out of its anchor on fake organisms underwater. The anchoring experiment is set up in **(a)** to pull robot out of the organism. Anchoring result in **(b)** for each organism contains seven trials, and the force gauge has an accuracy of 0.5 N.

water tank. Hexapus was placed above each object and all arms were actuated in flexion to grasp the object.

After Hexapus anchored to each object, we pulled it off the object using a handheld force sensor to record peak pull-out forces, with seven trials on each substrate (Fig. 8a, b). Surprisingly, the flexible sea kelp yielded the highest anchoring force, likely because the flexible kelp and arms were able to intertwine, and the arms could reach full flexion. The rigid coral objects yielded reasonable anchoring forces of at least 5 N. The soft artificial sea anemone performed the worst in anchoring because the structure was too small to enable entangling of the arms with the anemone.

### *Crawling*

To implement a crawling motion, we designed a control sequence that would enable actuators to propel Hexapus along the shallow ground, shown in Figure 9a and Supplementary Video S2. At the beginning of the crawling cycle, Hexapus maintains a crawling position, where the Dynamixel motor displaces all arms to $\sim 60°$ from their unactuated positions and all low-power motors displace arms' tips inward (120° deflection on the tip), forming a standing pose. Then three low-power DC motors facing the desired locomotion direction are simultaneously actuated and curl arms in flexion. Next, the other three

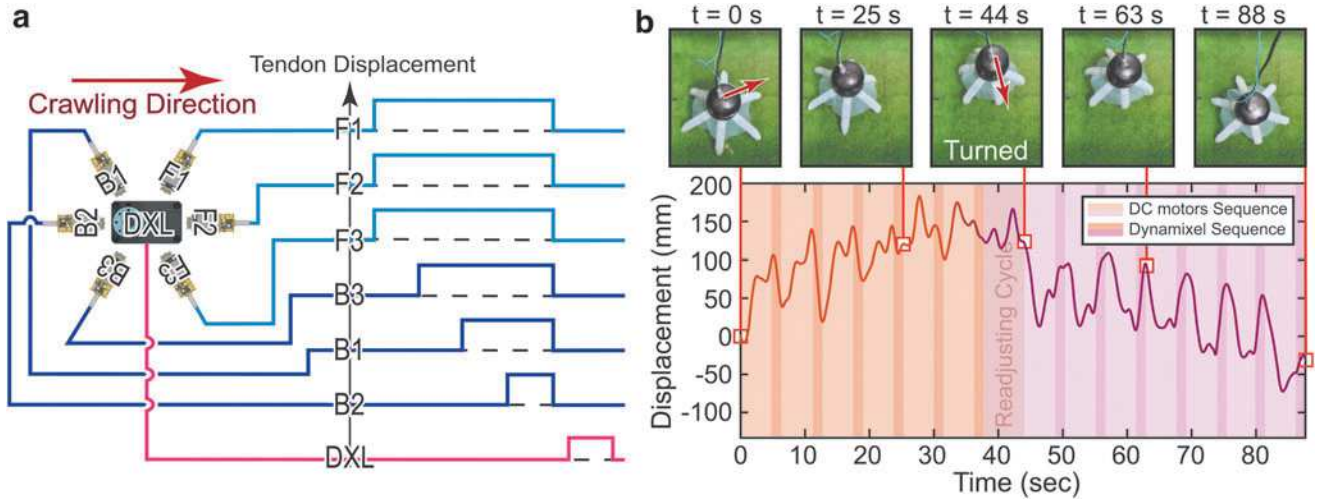


**FIG. 9.** Crawling sequence and performance. **(a)**. Proposed actuation sequence for crawling. The plot shows motors' position in a period of crawling, which is equivalent to displacements of their corresponding tendons from the initial crawling pose. Crawling direction is parallel to the arm controlled by low-power motor F2. **(b)**. Screenshots of the crawling demonstration at representative time stamps and distance traveled by robot. From $t = 0$ s to $t = 44$ s, the plot shows the distance of Hexapus from starting position at $t = 0$ s; after $t = 44$ s, the plot then shows the inverted and offset distance from $t = 44$ s.

arms are actuated in flexion sequentially. The timing of this actuation sequence drives the robot forward by creating asymmetric friction with the ground. This sequence gives each crawling cycle 6.25 s and walking direction resolution of 60° because each low-power motor can act as the front motor.

The crawling motion was tested in a 0.25 m deep water environment. Hexapus first performs crawling along one direction for six cycles, and then it changes direction by 120° and crawls for seven more cycles (Fig. 9b and Supplementary Video S2). We report that Hexapus is able to crawl at ~3.4 mm/s on a grass terrain.

## Discussion

This article introduces the design, fabrication, and performance of Hexapus, an integrated high-DOF underwater soft robot. Our robot Hexapus utilizes soft arms that enable it to perform multifunctional tasks, suggesting promising maneuverability, utility, and robustness. As a result of the hierarchical actuation that divides power strategically among actuators, Hexapus can perform low-cost-of-transport locomotion along with complicated maneuvering and tasks such as turning when transporting, grasping when crawling, and capturing (grasping) when anchoring. These functionalities achieved by energy-efficient actuations make Hexapus a good candidate for unmanned underwater operations such as explorations and transportation.

To demonstrate the effectiveness of Hexapus' functionalities in an underwater operation, we performed an exploration, sample, and return behavior. After transporting a sample to the surface, Hexapus swims backward to another location of the kelp cluster and finally anchors onto it to await next operation. Hexapus performed forward and backward swimming, turning, grasping, and anchoring throughout the demonstration, and the fast-responding turning, firm grasping, secure anchoring demonstrate the multifunctional capabilities of this robot (Supplementary Video S3 and Supplementary Fig. S3).

There has been extensive work developing octopus-inspired actuators and full mobile robot platforms.[32,33,35,54] Many of these robots use similar tendon-based actuation of their arms, and several of these robots have significantly more actuated DOF per arm compared with Hexapus.[55,56] In specific, the functionalities achieved by Hexapus are similar to those of other jellyfish robots such as that demonstrated in Ren et al.,[31] but in a different fluid dynamic and with interlimb control for turning and grasping. With a waterproof body containing all on-board controllers and actuators, Hexapus shows its unique potential for effective and autonomous underwater locomotion. In summary, Hexapus has demonstrated multimodal locomotion capabilities, including efficient swimming locomotion, promising maneuverability, and operational capability in various underwater terrains, all of which suggest its suitability in environment-friendly underwater operations.

Overall, the challenge and potential of multimodal actuation remain an area of constant improvement in soft robotics. Mobile platforms present some of the most exciting areas for soft robotics as they can explore, monitor, and interact with protected environments and living organisms.[57] Inspired by previous robot design studies, which differentially allocate actuators across DOF,[42–44] we envision that our design principle of hierarchical actuation can be applied across a broad range of mobile robot morphology for efficient, multifunctional behaviors. Thus, through continued development of new and efficient actuators, power sources, and critical design principles that balance efficiency and capabilities, we may realize fully mobile soft robots capable of deployment and operation in the wild.

## Author Disclosure Statement

No competing financial interests exist.

## Funding Information

This work was supported by the National Science Foundation under Grant No. (1935324) and by the Office of Naval Research under grant number N00014-20-1-2373.

## Supplementary Material

Supplementary Data S1
Supplementary Figure S1
Supplementary Figure S2
Supplementary Figure S3
Supplementary Figure S4
Supplementary Video S1
Supplementary Video S2
Supplementary Video S3

## References

1. Yang G-Z, Bellingham J, Dupont PE, et al. The grand challenges of science robotics. Sci Robot 2018;3(14): eaar7650.
2. Ren K, Yu JC. Research status of bionic amphibious robots: A review. Ocean Eng 2021;227:108862.
3. Giorgio-Serchi F, Arienti A, Corucci F, et al. Hybrid parameter identification of a multi-modal underwater soft robot. Bioinspir Biomim 2017;12(2):025007.
4. Pope MT, Kimes CW, Jiang H, et al. A multimodal robot for perching and climbing on vertical outdoor surfaces. IEEE Trans Robot 2016;33(1):38–48.
5. Kim K, Spieler P, Lupu E-S, et al. A bipedal walking robot that can fly, slackline, and skateboard. Sci Robot 2021; 6(59):eabf8136.
6. Crespi A, Karakasiliotis K, Guignard A, et al. Salamandra robotica II: An amphibious robot to study salamander-like swimming and walking gaits. IEEE Trans Robot 2013; 29(2):308–320.
7. Shin WD, Park J, Park H-W. Development and experiments of a bio-inspired robot with multi-mode in aerial and terrestrial locomotion. Bioinspir Biomim 2019;14(5):056009.
8. Jin H, Dong E, Alici G, et al. A starfish robot based on soft and smart modular structure (SMS) actuated by SMA wires. Bioinspir Biomim 2016;11(5):056012.
9. Shapiro A, Greenfield A, Choset H. Frictional compliance model development and experiments for snake robot climbing. In: Proceedings 2007 IEEE International Conference on Robotics and Automation. IEEE: Rome, Italy; 2007; pp. 574–579.
10. Shen W-M, Krivokon M, Chiu H, et al. Multimode locomotion via superbot reconfigurable robots. Auton Robots 2006;20(2):165–177.
11. Zhao J, Cui X, Zhu Y, et al. UBot: A new reconfigurable modular robotic system with multimode locomotion ability. Ind Robot Int J 2012;39(2):178–190.
12. Brunete A, Ranganath A, Segovia S, et al. Current trends in reconfigurable modular robots design. Int J Adv Robot Syst 2017;14(3):1729881417710457.

13. Yim M, Shen W-M, Salemi B,et al. Modular self-reconfigurable robot systems [grand challenges of robotics]. IEEE Robot Autom Mag 2007;14(1):43–52.
14. Russo S, Harada K, Ranzani T, et al. Design of a robotic module for autonomous exploration and multimode locomotion. IEEE/ASME Trans Mechatron 2012;18(6):1757–1766.
15. Booth JW, Shah D, Case JC, et al. Omniskins: Robotic skins that turn inanimate objects into multifunctional robots. Sci Robot 2018;3(22):eaat1853.
16. Rus D, Tolley MT. Design, fabrication and control of soft robots. Nature 2015;521(7553):467.
17. Shah D, Yang B, Kriegman S, et al. Shape changing robots: Bioinspiration, simulation, and physical realization. Adv Mater 2021;33(19):2002882.
18. Shah DS, Yuen MC, Tilton LG, et al. Morphing robots using robotic skins that sculpt clay. IEEE Robot Autom Lett 2019;4(2):2204–2211.
19. Hu W, Lum GZ, Mastrangeli M, et al. Small-scale soft-bodied robot with multimodal locomotion. Nature 2018; 554(7690):81–85.
20. Shepherd RF, Ilievski F, Choi W, et al. A multi-gait soft robot supporting information. Multigait Soft Robot 2011; 108(51):20400–20403.
21. Anderson IA, Gisby TA, McKay TG, et al. Multi-functional dielectric elastomer artificial muscles for soft and smart machines. J Appl Phys 2012;112(4):041101.
22. Zhang S, Ke X, Jiang Q, et al. Programmable and reprocessable multifunctional elastomeric sheets for soft origami robots. Sci Robot 2021;6(53):eabd6107.
23. Christianson C, Cui Y, Ishida M, et al. Cephalopod-inspired robot capable of cyclic jet propulsion through shape change. Bioinspir Biomim 2020;16(1):016014.
24. Katzschmann RK, DelPreto J, MacCurdy R, et al. Exploration of underwater life with an acoustically controlled soft robotic fish. Sci Robot 2018;3(16):eaar3449.
25. Serchi FG, Arienti A, Baldoli I, et al. An elastic pulsed-jet thruster for soft unmanned underwater vehicles. In: 2013 IEEE International Conference on Robotics and Automation. IEEE: Karlsruhe, Germany; 2013; pp. 5103–5110.
26. Najem J, Sarles SA, Akle B, et al. Biomimetic jellyfish-inspired underwater vehicle actuated by ionic polymer metal composite actuators. Smart Mater Struct 2012;21(9): 094026.
27. Shintake J, Cacucciolo V, Shea H, et al. Soft biomimetic fish robot made of dielectric elastomer actuators. Soft Robot 2018;5(4):466–474.
28. Villanueva A, Bresser S, Chung S, et al. Jellyfish inspired underwater unmanned vehicle. In: Society of Photo-Optical Instrumentation Engineers (SPIE) Conference Series, vol. 7287. (Bar-Cohen Y, Wallmersperger T. eds.) Society of Photo-Optical Instrumentation Engineers (SPIE): San Diego, California, US; 2009; p. 72871G.
29. Bujard T, Giorgio-Serchi F, Weymouth G. A resonant squid-inspired robot unlocks biological propulsive efficiency. Sci Robot 2021;6(50):eabd2971.
30. Joshi A, Kulkarni A, Tadesse Y. Fludojelly: Experimental study on jellyfish-like soft robot enabled by soft pneumatic composite (SPC). Robotics 2019;8(3):56.
31. Ren Z, Hu W, Dong X, et al. Multi-functional soft-bodied jellyfish-like swimming. Nature Commun 2019;10(1):1–12.
32. Arienti A, Calisti M, Giorgio-Serchi F, et al. Poseidrone: Design of a soft-bodied ROV with crawling, swimming and manipulation ability. In: 2013 OCEANS-San Diego. IEEE: San Diego, CA, USA; 2013; pp. 1–7.
33. Laschi C, Cianchetti M, Mazzolai B, et al. Soft robot arm inspired by the octopus. Adv Robot 2012;26(7):709–727.
34. Fras J, Noh Y, Macias M, et al. Bio-inspired octopus robot based on novel soft fluidic actuator. In: 2018 IEEE International Conference on Robotics and Automation (ICRA). IEEE: Brisbane, QLD, Australia; 2018; pp. 1583–1588.
35. Shen Z, Na J, Wang Z. A biomimetic underwater soft robot inspired by cephalopod mollusc. IEEE Robot Autom Lett 2017;2(4):2217–2223.
36. Almubarak Y, Schmutz M, Perez M, et al. Kraken: A wirelessly controlled octopus-like hybrid robot utilizing stepper motors and fishing line artificial muscle for grasping underwater. Internat J Intell Robotic Applcat 2021;6(3): 543–563.
37. Cianchetti M, Calisti M, Margheri L, et al. Bioinspired locomotion and grasping in water: the soft eight-arm octopus robot. Bioinspir Biomim 2015;10(3):035003.
38. Shen Q, Olsen Z, Stalbaum T, et al. Basic design of a biomimetic underwater soft robot with switchable swimming modes and programmable artificial muscles. Smart Mater Struct 2020;29(3):035038.
39. Sfakiotakis M, Kazakidi A, Chatzidaki A, et al. Multi-arm robotic swimming with octopus-inspired compliant web. In: 2014 IEEE/RSJ International Conference on Intelligent Robots and Systems. IEEE: Chicago, IL, USA; 2014; pp. 302–308.
40. Li T, Nakajima K, Calisti M, et al. Octopus-inspired sensorimotor control of a multi-arm soft robot. In: 2012 IEEE International Conference on Mechatronics and Automation. IEEE: Chengdu, China; 2012; pp. 948–955.
41. Shi L, Guo S, Asaka K. A novel multifunctional underwater microrobot. In: 2010 IEEE International Conference on Robotics and Biomimetics. IEEE: Tianjin, China; 2010; pp. 873–878.
42. Zinn MR, Roth B, Khatib O, et al. A new actuation approach for human friendly robot design. Int J Robot Res 2004;23(4–5):379–398.
43. Shin D, Sardellitti I, Park Y-L, et al. Design and control of a bio-inspired human-friendly robot. Int J Robot Res 2010; 29(5):571–584.
44. Bowling A. Macro-mini Manipulation. In: Encyclopedia of Robotics (Ang M, Khatib O, Siciliano, B. eds.) Springer: Berlin, Heidelberg; 2020; pp. 1–5.
45. Feitl KE, Millett AF, Colin SP, et al. Functional morphology and fluid interactions during early development of the scyphomedusa aurelia aurita. Biol Bull 2009;217(3):283–291.
46. Jiang M, Zhou Z, Gravish N. Flexoskeleton printing enables versatile fabrication of hybrid soft and rigid robots. Soft Robot 2020;7(6):770–778.
47. Yu Q, Jiang M, Gravish N. Flexoskeleton fingers: 3d printed reconfigurable ridges enabling multi-functional and low-cost underactuated grasping. IEEE Robot Autom Lett 2021;6(2):3971–3978.
48. Baldwin J, England WR. A comparison of anaerobic energy metabolism in mantle and tentacle muscle of the blue-ringed octopus, *Hapalochlaena maculosa*, during swimming. Aust J Zool 1980;28(3):407–412.
49. Boyraz P, Runge G, Raatz A. An Overview of Novel Actuators for Soft Robotics. In: Actuators, vol. 7. Multidisciplinary Digital Publishing Institute: Basel, Switzerland; 2018; p. 48.
50. Cho JH, Richards RF, Bahr DF, et al. Efficiency of energy conversion by piezoelectrics. Appl Phys Lett 2006; 89(10):104107.

51. McHenry MJ, Jed J. The ontogenetic scaling of hydrodynamics and swimming performance in jellyfish (*Aurelia aurita*). J Exp Biol 2003;206(22):4125–4137.
52. Villanueva A, Smith C, Priya S. A biomimetic robotic jellyfish (robojelly) actuated by shape memory alloy composite actuators. Bioinspir Biomim 2011;6(3):036004.
53. O'dor RK. Respiratory metabolism and swimming performance of the squid, loligo opalescens. Can J Fish Aquat Sci 1982;39(4):580–587.
54. Nguyen DQ, Ho VA. Anguilliform swimming performance of an eel-inspired soft robot. Soft Robot 2021;9(3):425–439.
55. Renda F, Giorelli M, Calisti M, et al. Dynamic model of a multibending soft robot arm driven by cables. IEEE Trans Rob 2014;30(5):1109–1122.
56. Laschi C, Mazzolai B, Mattoli V, et al. Design of a biomimetic robotic octopus arm. Bioinspir Biomim 2009;4(1):015006.
57. Rich SI, Wood RJ, Majidi C. Untethered soft robotics. Nat Electron 2018;1(2):102–112.

Address correspondence to:
*Nick Gravish*
*Mechanical and Aerospace Engineering*
*University of California San Diego*
*9500 Gilman Drive*
*La Jolla, CA 92093*
*USA*

*E-mail:* ngravish@eng.ucsd.edu